NANO LETTERS

Letter

pubs.acs.org/NanoLett

Anisotropy of the Thermal Conductivity in GaAs/AlAs Superlattices

Maria N. Luckyanova,[†] Jeremy A. Johnson,[‡] A. A. Maznev,[‡] Jivtesh Garg,[†] Adam Jandl,[§] Mayank T. Bulsara,[§] Eugene A. Fitzgerald,[§] Keith A. Nelson,[‡] and Gang Chen*,[†]

[†]Department of Mechanical Engineering, [‡]Department of Chemistry, and [§]Department of Materials Science and Engineering, Massachusetts Institute of Technology, Cambridge, Massachusetts 02139, United States

ABSTRACT: We combine the transient thermal grating and time-domain thermoreflectance techniques to characterize the anisotropic thermal conductivities of GaAs/AlAs superlattices from the same wafer. The transient grating technique is sensitive only to the in-plane thermal conductivity, while time-domain thermoreflectance is sensitive to the thermal conductivity in the cross-plane direction, making them a powerful combination to address the challenges associated with characterizing anisotropic heat conduction in thin films. We compare the experimental results from the GaAs/AlAs superlattices with first-principles calculations and previous measurements of Si/Ge SLs. The measured anisotropy is smaller than that of Si/Ge SLs, consistent with both the mass-mismatch picture of interface scattering and with the results of calculations from density-functional perturbation theory with interface mixing included.

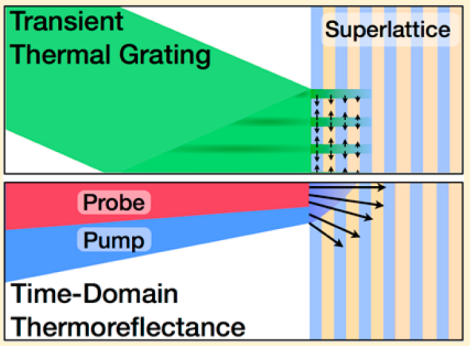

KEYWORDS: *Nanoscale heat conduction, superlattice, thermal conductivity anisotropy, time-domain thermoreflectance, transient thermal grating*

The thermal properties of superlattices (SLs) are of great interest in a range of fields. Due to their decreased thermal conductivities, SLs are an important fundamental learning tool for developing better thermoelectric energy conversion materials.[1,2] In optoelectronics, SLs often serve as the gain media or the mirrors in solid-state semiconductor lasers, even though their low aggregate thermal conductivities often lead device temperatures to rise, degrading performance.[3] SLs are expected to have anisotropic thermal properties, resulting from both the modified phonon dispersion[4,5] and increased diffuse scattering of phonons at the interfaces.[6,7] So far, only a few studies have been conducted on the anisotropy of Si/Ge SLs by using the 3ω method and varying the linewidths of the heaters placed on Si/Ge SLs.[8−11] Measuring the thermal conductivity anisotropy of SLs has proven challenging because frequently used techniques such as the 3ω method[12] and optical pump−probe[13] are more sensitive to cross-plane thermal transport.[14] Measurements of in-plane thermal properties using ac calorimetry rely on freestanding films.[15,16] The two-wire 3ω method characterizes thermal conductivity anisotropy of SLs by using two heaters of different widths, with one being much wider than the thin film thickness so that its temperature rise is independent of the in-plane thermal conductivity of the film. The other heater has a width smaller than or comparable to the film thickness, such that its temperature rise depends on heat spreading laterally inside the film, making it sensitive to the in-plane thermal conductivity. However, due to the dominance of the cross-plane thermal conductivity in determining both heaters' temperature rise, the sensitivity to the in-plane thermal conductivity is limited and depends on the film thickness as well as the thermal conductivity anisotropy.[10] Extensive theoretical and modeling studies[17,18] have been carried out on heat conduction mechanisms in SLs using lattice dynamics[4,19] and molecular dynamics simulations.[20] Continued experimental and theoretical studies deepen our understanding of the heat conduction mechanisms in SLs, which serve as excellent platforms to explore and engineer nanoscale phonon heat conduction.[21] Experimental tools capable of measuring the anisotropic thermal conductivity of SLs, and thin films in general, are needed. In this paper, we combine the transient thermal grating (TTG) and time-domain thermoreflectance (TDTR) techniques to characterize anisotropic thermal conductivity. Using this combination, we report the anisotropic thermal conductivity of GaAs/AlAs SLs and compare the experimental results with first-principles calculations and previous measurements of thermal conductivity anisotropy in Si/Ge SLs.

We used two noninvasive optical techniques in tandem to measure the anisotropic thermal properties of two GaAs/AlAs SLs grown with metal organic chemical vapor deposition (MOCVD). The TDTR technique[13,14,22] was used to measure the cross-plane thermal conductivities, and TTG[23−29] measured the in-plane thermal diffusivities. These two techniques have not been combined before to characterize the anisotropy of thermal transport in thin films and SLs. Both techniques use lasers to induce a temperature rise at the sample surface and to monitor the temperature decay via heat conduction. The main difference between the two techniques lies in the spatial distribution of the excitation laser light at the sample surface, as illustrated in Figure 1A and B. In TDTR (Figure 1A), we used a

Received: January 10, 2013
Revised: August 7, 2013
Published: August 16, 2013

   dx.doi.org/10.1021/nl4001162 | *Nano Lett.* 2013, 13, 3973−3977

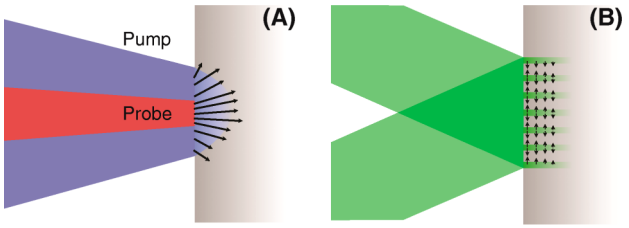

Figure 1. Schematic diagram of the laser excitation and subsequent heat diffusion pathways due to (A) the time-domain thermoreflectance (TDTR) setup and (B) the transient thermal grating (TTG) setup.

large (60 μm) laser spot; hence on short time scales the heat transfer occurs primarily in the cross-plane direction. In TTG (Figure 1B), two interfering beams created a sinusoidal intensity pattern with a small period (on the order of a few micrometers). The heat transport in TTG occurs in both the in-plane and the cross-plane directions; however, as will be explained below, the temporal signature of the thermal grating decay is only sensitive to the in-plane thermal conductivity. This unique characteristic of the measurement was recognized only recently.[26] By combining the TDTR and TTG techniques, we measured the room temperature anisotropic thermal conductivity of GaAs/AlAs SLs and compared the results with previously reported measurements of cross- and in-plane conductivities on different GaAs/AlAs SLs. The results are also compared to first-principles calculations of SL thermal conductivity, accounting for both intrinsic and extrinsic phonon scattering channels, and contrasted with experimental data on Si/Ge superlattices, which have a larger acoustic mismatch.

Two 3.5 μm thick GaAs/AlAs SLs, an 8 nm × 8 nm (with a total period of 16 nm) SL and a 2 nm × 2 nm (with a total period of 4 nm) SL, were epitaxially grown by MOCVD on the [100] direction of a GaAs wafer with a 500 nm GaAs buffer. X-ray diffraction performed on the samples confirmed both the planarity and the period thicknesses of 4 and 16 nm for the two SL samples. For the TDTR measurements, a 90 nm Al optical-thermal transducer layer was deposited with e-beam evaporation.[30]

In the TDTR pump−probe measurements, a pump laser pulse (pulse duration 200 fs, wavelength 400 nm, spot size 60 μm, repetition rate 80 MHz, modulation frequency 3−12 MHz) impinged upon the sample, generating hot electrons in the metal transducer layer. The hot electrons quickly thermalized through electron−phonon interactions. Since the pump spot size is much larger than the thermal penetration depth, the resulting heat input propagated from the metal layer into the SL primarily in a direction perpendicular to the SL interfaces. A time-delayed probe pulse (pulse duration 200 fs, wavelength 800 nm, spot size 10 μm, repetition rate 80 MHz) measured the transient reflectivity of the surface of the metal transducer. This surface reflectivity is directly related to the surface temperature via the thermoreflectance coefficient. The resulting cooling curve (Figure 2A) was fit to a three-layer thermal diffusion model of the cooling of the sample. The layer structure consists of a thin metallic film, a finite thermal interface conductance between the metal transducer and the SL, and an anisotropic SL layer with an adiabatic back boundary. Fourier's law dictates the flow of heat within the metal transducer film and within the SL and is given by

$$C_i \frac{\partial T_i(z,t)}{\partial t} = k_i \frac{\partial^2 T_i(z,t)}{\partial z^2} \quad (1)$$

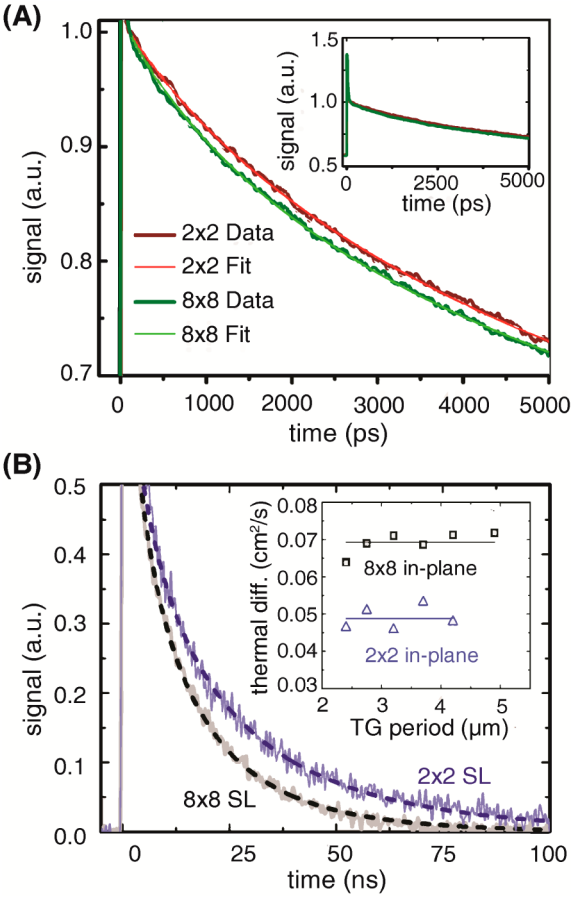

Figure 2. (A) TDTR and (B) TTG data and fits for the two SLs. The inset in B shows the thermal diffusivities of the two SLs at varying TG periods.

where C_i is the heat capacity and k_i is the cross-plane thermal conductivity of the layer i. There is a finite thermal resistance between the Al optical-thermal transducer layer and the SL due to the Kapitza conductance, G, given by

$$C_{Al} d \frac{\partial T_{Al}(z=d,t)}{\partial t} = -G[T_{Al}(z=d,t) - T_s(z=0,t)] \quad (2)$$

where C_{Al} is the aluminum heat capacity, d the thickness of the Al, T_{Al} is the temperature of the film, and T_s is the temperature of the SL. A multiparameter optimization was used to deduce the two unknown quantities: the thermal conductivity of the SL and the thermal interface conductance between the Al and the SL. The details of the experimental technique and data analysis have been discussed elsewhere.[14,22,31]

The in-plane thermal conductivity was measured using a transient thermal grating (TTG) technique. In the reflectance mode of this technique, two excitation pulses (pulse duration 60 ps, wavelength 515 nm, spot size 600 μm, repetition rate 1 kHz) interfered with each other on the surface of the sample to create a sinusoidal intensity profile with spacing L on the order of several micrometers. Absorption led to a spatially periodic heating and a resulting spatially periodic variation in the sample optical properties, forming a transient diffraction grating that encoded the material thermal response. A diffracted quasi-cw probe beam (wavelength 532 nm, spot size 300 μm), superposed with a reference beam in a heterodyne detection scheme,[26−28] was monitored to measure the temperature

dx.doi.org/10.1021/nl4001162 | Nano Lett. 2013, 13, 3973−3977

dynamics. Approximately 300 measurements were conducted per second so each resulting signal decay (Figure 2B) represents the average of 10 000 traces.

In general, the diffracted beam intensity was sensitive to both surface displacement and temperature "gratings" whose distinct time dependences can complicate the analysis of the diffracted signal decay measured in the reflection geometry. Heterodyne phase control was used to eliminate the surface displacement component which only contributes to the signal through its effect on the optical phase.[26] Thus the signal decay that we measured (Figure 2B) tracked the dynamics of the amplitude of the spatially sinusoidal temperature grating at the sample surface.

The solution of the thermal diffusion equation[17] yields the following equation for the dynamics of the thermal grating decay at the surface $z = 0$:

$$T(z = 0, x, t) = T_0 e^{\alpha_z \zeta^2 t} \mathrm{efrc}(\zeta \sqrt{\alpha_z t}) \cos(qx) e^{-\alpha_x q^2 t} \quad (3)$$

where ζ is the optical absorption coefficient, $q = 2\pi/L$ is the wave vector magnitude of the thermal grating, α_z and α_x are the cross-plane and in-plane thermal diffusivity values, respectively, and erfc is the complementary error function. The decay is influenced by both cross- and in-plane diffusivities; however, the former only affects the initial shape of the decay; at long times $t > \alpha_z^{-1}\zeta^{-2}$ and eq 3 takes the asymptotic form

$$T(z = 0, x, t) = \frac{T_0}{\pi^{1/2}\zeta} (\alpha_z t)^{-1/2} \cos(qx) e^{-\alpha_x q^2 t} \quad (4)$$

The temporal profile of the signal decay is completely determined by α_x, while α_z only affects the amplitude factor. Thus the TTG method is selectively sensitive to the in-plane diffusivity unlike the TDTR or 3ω methods which, depending on the configuration, are sensitive to either both in- and cross-plane thermal conductivities or primarily to the cross-plane conductivity. This unique characteristic makes the TTG technique ideally suited to characterize the in-plane thermal conductivities of superlattices. In our SL samples, we estimate the absorption coefficient at the excitation wavelength to be $\sim 4 \times 10^4$ cm^{-1}. Consequently, the cross-plane diffusivity influences the decay dynamics only at short times, $t \leq 10$ ns. Indeed, Figure 2B shows that the measured decay curves can be accurately fit with eq 4 for $t > 10$ ns.

Equations 3 and 4 are obtained for a uniform anisotropic half-space and do not account for the presence of the substrate. This is justified as long as the thermal grating decays before it can extend deeply enough to reach the substrate. The thermal penetration depth into the substrate is given by $h \sim 2(\alpha_z t)^{1/2}$. Considering that the time window used for the data analysis was 10−150 ns, let us take $t = 150$ ns; with the highest value of α_z measured using the TDTR method we get $h \sim 1.8$ μm, significantly shorter than the SL thickness of 3.5 μm. For a longer TTG period, the time window of the experiment would be longer in order to allow in-plane heat transport from grating peak to null, and thus the thermal penetration depth would increase. Since the GaAs substrate has a much higher diffusivity than the SL, we would expect the apparent diffusivity to go up with a longer grating period if the substrate effect becomes significant. However, for the TTG period range used in our measurements, 2.5−5 μm, the diffusivity was nearly constant, as shown in the inset in Figure 2B, giving us another indication that the substrate effect is negligible.

In the TTG method, in contrast with the TDTR method, we do not use a metal coating. This is an important difference that deserves a brief discussion. Measuring an uncoated sample entails a number of advantages: no sample preparation is required and the measurements are affected neither by the metal film thickness nor by the thermal boundary resistance at the metal−semiconductor interface.[13] Thus, there is no need to employ multiparameter fitting. In fact, in the model we use to fit the data, given by eq 4, the only variable parameter is the parameter of interest. On the other hand, photothermal measurements on uncoated semiconductors are often complicated by the presence of photoexcited carriers.[32] Indeed, laser excitation creates both a temperature grating and a concentration grating of the excited carriers with the latter also influencing the refractive index and contributing to diffraction of the probe beam. However, the ambipolar diffusion coefficient of photoexcited carriers in both bulk GaAs[33] and GaAs quantum wells[34] exceeds 10 cm^2/s, whereas the thermal diffusivity measured on our samples is well below 0.1 cm^2/s. Consequently, the carrier grating should decay much faster than the thermal grating. Indeed, we do observe a small initial spike of duration ∼0.5 ns limited by the resolution of the detection electronics, which may be caused by the photoexcited carriers. On the longer time scale of interest the carrier contribution should be entirely negligible, which is confirmed by the fact that the thermal model alone generally fits the data very well.

The above discussion makes it clear that the combination of the TDTR and TTG methods is a powerful solution to the challenge of determining the anisotropic thermal conductivity of thin films and is ideally suited for studying the physics of phonon heat conduction in SLs. Figure 2A shows raw data and the corresponding fitting curves from the TDTR experiment for the SLs we studied. Figure 2B shows the data and fitting for the TTG experiment at four different grating periods. The solid lines are measured data, and the dashed lines are fittings to the data with eq 4.

The experimental in-plane and cross-plane thermal conductivities as well as the resulting anisotropies are given in Table 1. The anisotropy is defined as the in-plane thermal conductivity divided by the cross-plane thermal conductivity.

Table 1. Calculated and Experimentally Measured Thermal Conductivities and Anisotropies for 2 nm × 2 nm and 8 nm × 8 nm GaAs/AlAs SLs (296 K), Measured with TDTR and TTG, and 2 nm × 2 nm Si/Ge SLs (260 K), Measured with the 3ω Method[9]

SL layer thickness	2 nm	8 nm
GaAs/AlAs in-plane α_x (cm^2/s), experimental	0.0488	0.0693
GaAs/AlAs in-plane k_x (W/m·K), exptl	8.05 ± 0.48	11.4 ± 0.46
GaAs/AlAs in-plane k_x (W/m·K), calculated	18.64	
GaAs/AlAs cross-plane k_z (W/m·K), exptl	6.5 ± 0.5	8.7 ± 0.4
GaAs/AlAs cross-plane k_z (W/m·K), calcd	15.0	
GaAs/AlAs anisotropy, exptl	1.2 ± 0.12	1.3 ± 0.08
GaAs/AlAs anisotropy, calcd	1.24	
Si/Ge in-plane k_x (W/m·K), exptl[9]	6.3	
Si/Ge cross-plane k_z (W/m·K), exptl[9]	1.6	
Si/Ge in-plane k_x (W/m·K), calcd[36]	9.35	
Si/Ge cross-plane k_z (W/m·K), calcd[36]	5.02	
Si/Ge SL anisotropy, exptl[9]	3.9	
Si/Ge SL anisotropy, calcd[36]	1.9	

dx.doi.org/10.1021/nl4001162 | Nano Lett. 2013, 13, 3973−3977

Thermal conductivity, k, values in the table are obtained from experimentally measured thermal diffusivities via $k = \alpha\rho c_p$, where c_p is the average of the specific heats of GaAs and AlAs and ρ is the average of their densities.[35] For the TDTR experiments, each SL was measured at five different locations under four different pump modulation frequencies. No systematic frequency dependence was found. Thus, the thermal conductivities given represent the averages of 20 measurements and the standard deviation of these measurements. The error given for the TTG measurements is the standard deviation in the five grating spacing measurements shown in the inset of Figure 2B. The thermal conductivities are lower than the corresponding bulk values. The table also shows the values for in- and cross-plane thermal conductivities in 2 nm × 2 nm Si/Ge symmetrically strained SLs as well as the resulting anisotropy, obtained using the 3ω method with two different heater widths.[9] The results indicate that the anisotropy is significantly higher in the Si/Ge SLs due to the larger mass difference and corresponding mismatch in the phonon properties between the Si and Ge layers, compared to that between GaAs and AlAs layers.

A comparison of our results from these experiments with previously reported measurements for GaAs/AlAs SL thermal conductivities is shown in Figure 3.[15,30,37] The new data fit in well with the general trend of increasing thermal conductivities with increasing GaAs/AlAs SL period thickness. Variations among data reported by different authors are expected because phonon mean free paths (MFPs) in SLs are strongly influenced by defect scattering and interface roughness[6,7] which could vary depending on the fabrication process. Since previous in-plane and cross-plane data were obtained on different samples, they do not provide reliable information about the thermal conductivity anisotropy in a given material system.

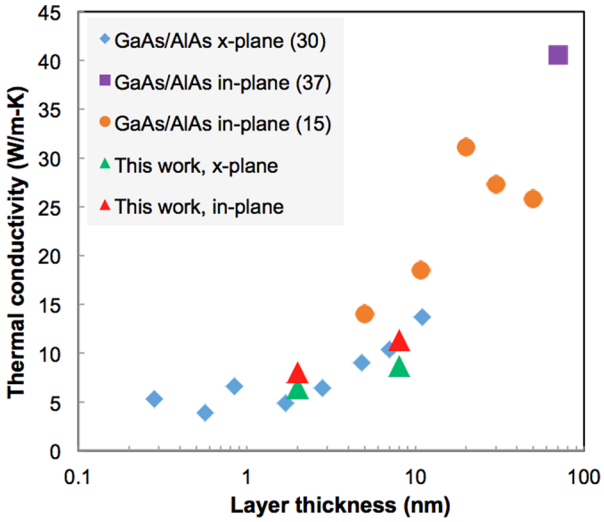

Figure 3. A comparison of the values of GaAs/AlAs thermal conductivities from the TDTR and TTG experiments with results from previous studies.

The reduced thermal conductivity can be understood as a consequence of additional phonon scattering due to interface roughness. In the past, such interface roughness has been modeled under the particle picture of phonon transport as causing partially diffuse and partially specular phonon scattering at the interfaces[6,7] or with molecular dynamics simulations.[4] We have performed first principles calculations of the thermal conductivities of GaAs/AlAs and Si/Ge SLs using density functional perturbation theory (DFPT), including the effects of atomic mixing at interfaces.[36−40] To compute the thermal conductivity from first principles, second-order and third-order interatomic force constants were derived using DFPT. The SL was then simulated by allocating the masses of Ga, Al, and As to the appropriate atoms in the unit cell. The calculation of in- and cross-plane thermal conductivities was performed both for SLs with perfect interfaces and SLs with atomistic mixing at interfaces but a fixed planarity. The atomistic mixing used in the simulations consisted of one monolayer on either side of the interface having randomly mixed Ga and Al atoms.[41] For perfect SLs, phonons scatter only through anharmonic three-phonon processes, and these scattering rates were computed using perturbation theory. Scattering from rough interfaces was computed by including random mass mixing in two atomic monolayers on either side of the interface. The thermal conductivities of the SLs were then calculated by solving the Boltzmann transport equation under the single-mode relaxation time approximation. Details of the simulation are published elsewhere.[21] The anisotropy was found to be higher in SLs with perfect interfaces (Figure 4). The smaller anisotropy values for rough interfaces more closely corresponded to experimental values. The simulated anisotropy for a Si/Ge SL (2 nm × 2 nm) with interface mixing is approximately 1.9, in reasonable agreement with the experimentally determined value.[36] Furthermore, the results show why the thermal conductivity anisotropy of GaAs/AlAs SLs is lower than that of Si/Ge SLs, where an increased mass mismatch leads to more scattering at the interfaces and a greater reduction in phonon group velocities. Due to computational power limits, the thermal conductivity of the 8 nm × 8 nm SL was not simulated. However, the experimental results for anisotropy are close to the simulated results for the 2 nm × 2 nm SL when atomistic mixing is included (Figure 4).

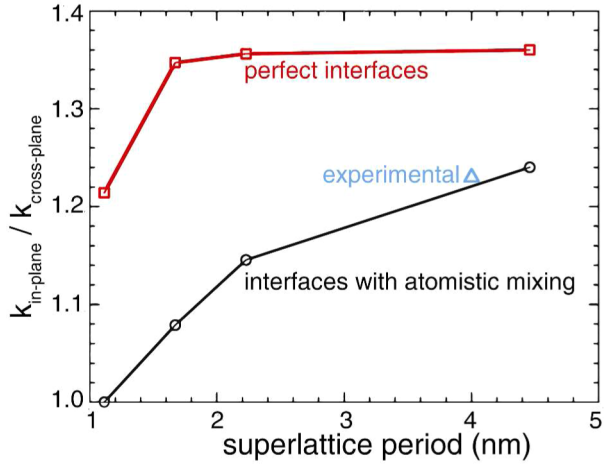

Figure 4. Anisotropy ratio of short period GaAs/AlAs superlattices. The ratio is lower when interfaces have atomic mixing and increases with increasing period.

However, the absolute values for thermal conductivity from the simulations, both in the in-plane and the cross-plane directions, are approximately two times higher than the experimentally determined thermal conductivities (Table 1). This may be the result of the model used in the calculations, wherein the interface roughness was approximated as random

dx.doi.org/10.1021/nl4001162 | Nano Lett. 2013, 13, 3973−3977

atomistic mixing, while real interface roughness in GaAs/AlAs SLs consists of both atomic mixing and local layer thickness fluctuations, also known as the formation of islands. The interface mixing is treated as a perturbation to perfect interfaces, essentially equivalent to that of point defects, resulting in a $\sim\omega^4$ frequency dependence of the scattering rates.[21] In this model, interface roughness predominantly affects high-frequency phonons while having little effect on the MFPs of low-frequency phonons. The local thickness fluctuations, which can have lateral dimensions ~10 nm,[42] can scatter long wavelength phonons. The additional island scattering picture is consistent with recent measurements of coherent phonon lifetimes in similar SL structures showing that extrinsic scattering rates of sub-THz phonons were indeed much larger than those predicted by the atomistic mixing model.[43] How to include both island formation and atomic mixing into DFPT simulations remains a challenge.

In summary, we have shown that the TTG technique is sensitive to the in-plane thermal conductivities of thin films and combined it with the TDTR technique to probe the anisotropies in the thermal conductivities of GaAs/AlAs SLs. The anisotropy in the thermal conductivities of GaAs/AlAs SLs is much smaller than that of the Si/Ge SLs reported in the past, consistent with pictures obtained from first-principles simulation. Although DFPT simulations produced similar anisotropy values compared to experimental data for both GaAs/AlAs and Si/Ge SLs, the thermal conductivity values predicted are about a factor of 2 higher than experiments, potentially due to local thickness fluctuations.

AUTHOR INFORMATION

Corresponding Author

*E-mail: gchen2@mit.edu.

Present Address

J.A.J.: Paul Scherrer Institut, Villigen, Switzerland.

Notes

The authors declare no competing financial interest.

ACKNOWLEDGMENTS

This material is based upon work supported as part of the Solid State Solar-Thermal Energy Conversion Center (S^3TEC), an Energy Frontier Research Center funded by the U.S. Department of Energy, Office of Science, Office of Basic Energy Sciences under Award Number DE-SC0001299/DE-FG02-09ER46577. M.N.L. was supported by the National Science Foundation Graduate Research Fellowship under Grant No. 1122374.

REFERENCES

(1) Chowdhury, I.; Prasher, R.; Lofgreen, K.; Chrysler, G.; Narasimhan, S.; Mahajan, R.; Koester, D.; Alley, R.; Venkatasubramanian, R. *Nat. Nanotechnol.* **2009**, *4*, 235−238.

(2) Venkatasubramanian, R.; Siivola, E.; Colpitts, T.; O'Quinn, B. *Nature* **2001**, *413*, 597−602.

(3) Faist, J.; Capasso, F.; Sivco, D. L.; Sirtori, C.; Hutchinson, A. L.; Cho, A. Y. *Science (New York, N.Y.)* **1994**, *264*, 553−556.

(4) Tamura, S.; Tanaka, Y.; Maris, H. J. *Phys. Rev. B* **1999**, *60*, 2627−2630.

(5) Hyldgaard, P.; Mahan, G. D. *Phys. Rev. B* **1997**, *56*, 10754−10757.

(6) Chen, G. *Phys. Rev. B* **1998**, *57*, 14958−14973.

(7) Chen, G. *J. Heat Transfer* **1997**, *119*, 220.

(8) Borca-Tasciuc, T.; Liu, W.; Liu, J.; Zeng, T.; Song, D. W.; Moore, C. D.; Chen, G.; Wang, K. L.; Goorsky, M. S.; Radetic, T.; Gronsky, R.; Koga, T.; Dresselhaus, M. S. *Superlattices Microstruct.* **2000**, *28*, 199−206.

(9) Liu, W. L.; Borca-Tasciuc, T.; Chen, G.; Liu, J. L.; Wang, K. L. *J. Nanosci. Nanotechnol.* **2001**, *1*, 39−42.

(10) Borca-Tasciuc, T.; Kumar, A. R.; Chen, G. *Rev. Sci. Instrum.* **2001**, *72*, 2139.

(11) Yang, B.; Liu, W. L.; Liu, J. L.; Wang, K. L.; Chen, G. *Appl. Phys. Lett.* **2002**, *81*, 3588.

(12) Cahill, D. G. *Rev. Sci. Instrum.* **1990**, *61*, 802.

(13) Capinski, W. S.; Maris, H. J. *Rev. Sci. Instrum.* **1996**, *67*, 2720.

(14) Schmidt, A. J.; Chen, X.; Chen, G. *Rev. Sci. Instrum.* **2008**, *79*, 114902.

(15) Yao, T. *Appl. Phys. Lett.* **1987**, *51*, 1798.

(16) Chen, G.; Tien, C. L.; Wu, X.; Smith, J. S. *J. Heat Transfer* **1994**, *116*, 325.

(17) Yang, B.; Chen, G. In *Thermal Conductivity: Theory, Properties, and Applications*; Tritt, T., Ed.; Kluwer Academic/Plenum Publishers: New York, 2004; pp 167−182.

(18) Luo, T.; Chen, G. *Phys. Chem. Chem. Phys.* **2013**, *15*, 3389−412.

(19) Simkin, M.; Mahan, G. *Phys. Rev. Lett.* **2000**, *84*, 927−30.

(20) Volz, S.; Saulnier, J. B.; Chen, G.; Beauchamp, P. *Microelectron. J.* **2000**, *31*, 815−819.

(21) Luckyanova, M. N.; Garg, J.; Esfarjani, K.; Jandl, A.; Bulsara, M. T.; Schmidt, A. J.; Minnich, A. J.; Chen, S.; Dresselhaus, M. S.; Ren, Z.; Fitzgerald, E. A.; Chen, G. *Science (New York, N.Y.)* **2012**, *338*, 936−9.

(22) Cahill, D. G.; Goodson, K.; Majumdar, A. *J. Heat Transfer* **2002**, *124*, 223.

(23) Rogers, J. A.; Maznev, A. A.; Banet, M. J.; Nelson, K. A. *Annu. Rev. Mater. Sci.* **2000**, *30*, 117−157.

(24) Graebner, J. E. *Rev. Sci. Instrum.* **1995**, *66*, 3903.

(25) Marshall, C. D.; Tokmakoff, A.; Fishman, I. M.; Eom, C. B.; Phillips, J. M.; Fayer, M. D. *J. Appl. Phys.* **1993**, *73*, 850.

(26) Johnson, J. A.; Maznev, A. A.; Bulsara, M. T.; Fitzgerald, E. A.; Harman, T. C.; Calawa, S.; Vineis, C. J.; Turner, G.; Nelson, K. A. *J. Appl. Phys.* **2012**, *111*, 023503.

(27) Goodno, G. D.; Dadusc, G.; Miller, R. J. D. *J. Opt. Soc. Am. B* **1998**, *15*, 1791−1794.

(28) Maznev, A. A.; Nelson, K. A.; Rogers, J. A. *Opt. Lett.* **1998**, *23*, 1319−21.

(29) Käding, O. W.; Skurk, H.; Maznev, A. A.; Matthias, E. *Appl. Phys. A: Mater. Sci. Process.* **1995**, *61*, 253−261.

(30) Capinski, W. S.; Maris, H. J.; Ruf, T.; Cardona, M.; Ploog, K.; Katzer, D. S. *Phys. Rev. B* **1999**, *59*, 8105.

(31) Capinski, W. S.; Maris, H. J. *Phys. B: Condens. Matter* **1996**, *219−220*, 699−701.

(32) Hurley, D. H.; Wright, O. B.; Matsuda, O.; Shinde, S. L. *J. Appl. Phys.* **2010**, *107*, 023521.

(33) Ruzicka, B. A.; Werake, L. K.; Samassekou, H.; Zhao, H. *Appl. Phys. Lett.* **2010**, *97*, 262119.

(34) Hillmer, H.; Forchel, A.; Tu, C. W. *Phys. Rev. B* **1992**, *45*, 1240−1245.

(35) Adachi, S. *GaAs and Related Materials*; World Scientific: River Edge, NJ, 1994; pp 15−30.

(36) Garg, J.; Chen, G. *Phys. Rev. B* **2013**, *87*, 140302.

(37) Yu, X. Y.; Chen, G.; Verma, A.; Smith, J. S. *Appl. Phys. Lett.* **1995**, *67*, 3554.

(38) Broido, D. A.; Malorny, M.; Birner, G.; Mingo, N.; Stewart, D. A. *Appl. Phys. Lett.* **2007**, *91*, 231922.

(39) Garg, J.; Bonini, N.; Kozinsky, B.; Marzari, N. *Phys. Rev. Lett.* **2011**, *106*, 045901.

(40) Bonini, N.; Garg, J.; Marzari, N. *Nano Lett.* **2012**, *12*, 2673.

(41) Robb, P. D.; Craven, A. J. *Ultramicroscopy* **2008**, *109*, 61−69.

(42) Bimberga, D.; Mars, D.; Miller, J. N.; Bauer, R.; Oertel, D.; Christen, J. *Superlattices Microstruct.* **1987**, *3*, 79−82.

(43) Hofmann, F.; Garg, J.; Maznev, A. A.; Jandl, A.; Bulsara, M.; Fitzgerald, E. A.; Chen, G.; Nelson, K. A. *J. Phys.: Condens. Matter* **2013**, *25*, 295401.